Analysis and optimisation of an axial flux permanent magnet coreless motor based on the field model using the superposition principle and genetic algorithm

RAFAŁ M. WOJCIECHOWSKI

Institute of Electrical Engineering and Electronics
Department of Mechatronics and Electrical Machines
Poznań University of Technology
Piotrowo 3A, 60-965 Poznań, Poland
e-mail: rafal.wojciechowski@put.poznan.pl

Abstract: In the paper, methodologies for the magnetic field simulation in an axial flux permanent magnet coreless (AFPMC) motor have been proposed and discussed. Two approaches have been considered and investigated, both based on representing the 3D field distribution by superimposing axisymmetric 2D patterns. The first of studied approaches applies directly to the Biot-Savart law while the second uses a 2D axisymmetric finite element method. The selected results of magnetic field distributions and electromagnetic torque characteristics for the considered AFPMC motor have been presented and compared with results obtained using the commercial FEM package 'Maxwell'. The elaborated algorithms have been incorporated into the design routines allowing multi-parameter optimisation of the considered motor construction.

Key words: axial flux permanent magnet motor, Biot-Savart law, finite element analysis, magnetic fields, superposition principle, genetic algorithm

1. Introduction

The axial flux permanent magnet machines (AFPM) have recently found a growing interest by many researchers' teams over the world. The key reasons are high efficiency, compact design and high torque density of those machines. From discussed above features AFPM machines can be found in applications such as direct drives of electrical vehicles [1], flywheel energy storages and pulse power generators [2, 3] and elevators drives [4]. Beside design and optimisation tasks related to the classical structures of AFPM the intensive studies on the novel coreless constructions are being reported. The designs with efficiency above 96% have been discussed inter alia in [5, 6]. The initial target applications of such machines have taken root in the military industry, however currently the axial flux permanent magnet coreless (AFPMC) motors have become more and more popular also in the civil applications. The main

difficulty in the study of such machines is lack of magnetic field symmetries that allow for applying simplified 2D models. Thus, for the need of magnetic field analysis in such machines the full 3D simulation is usually required, e.g. using the commercial FEM packages, such as Ansoft, Magnet, Opera, Maxwell or Comsol. The alternative to the use of commercial software can be the development of in-house algorithms benefiting from specific properties of the considered machine and thus justifying simplifications and therefore allowing simpler and faster modelling methods. The author found himself faced with a dilemma of choosing the proper kind of software when designing the AFPMC motor (Fig. 1). For the design calculation and analysis of 3D field distribution in the considered motor Author used the gained experience and developed own computer software. In the discussed case, the AFPMC motor can be treated as a magnetically linear and homogeneous system, enabling its superposition to be applied to component fields due to individual sources as magnets and coils in this instance. Moreover, the methodology can be simplified further by identification of additional symmetries of the system; for the studied motor the sources exhibit axial symmetry, for example, allowing analytical or 2D finite element solutions to be used.

In the paper the efficient methodology for 3D field modelling of coreless systems through superposition of axisymmetric 2D solutions is sought. The ultimate purpose was to incorporate such solutions into the design optimisation routines allowing the 3D field effects to be accounted for. Two algorithms have been developed and compared, one using the in-house 2D finite element simulations and another relying on the direct application of the Biot-Savart law. Selected results are presented and verified against 3D computations using the Maxwell 3D software. Comparisons of computing times are provided and benefits of the in-house approach are emphasized. The algorithms are then integrated into the design procedures; the particular objective assumed in the example was to maximize the ratio of torque over mass of the magnets.

2. The construction of an AFPMC motor

A 14 pole-pair low power motor has been designed and built. The construction of the motor has been illustrated in Fig. 1, whereas main dimensions have been given in Fig. 2. It is expected that the considered motor will operate in the speed range of 10.000-20.000 rpm in a system of control and automation with high dynamics. The stator of the motor is made of printed circuit board (PCB) laminate on the surface of which the 3 phase winding has been placed. The winding consists of 21 solenoidal coils and is connected into the star agreement. Each coil has 130 turns wound on a plastic bobbin. It has been assumed that the designed motor will be supplied from the DC voltage source equal to 12 V by the BLDC inverter. The rotor consists of the disc shape polyamide plate and 28 uniformly distributed cylindrical neodymium iron boron permanent magnets of type N38. The magnets have magnetic permeability close to that of the air. The rotor is fixed to a shaft. The gap between the magnets and the upper surface of the coils is 1 mm.
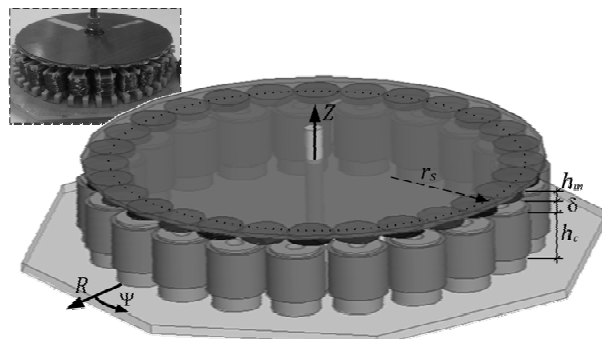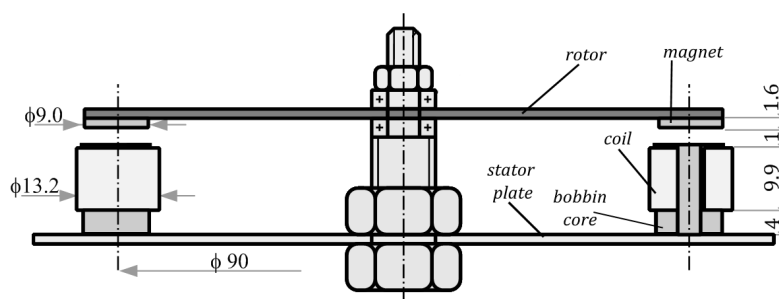
Fig. 1. View of the AFPMCM motor construction

Fig. 2. The main dimensions of the AFPMCM motor

3. The field models of AFPMC motor using superposition principle

In the considered AFPMC motor, where all components are either non-magnetic or may be assumed to have permeability close to that of air, superposition may be applied. Such approach offers a possibility of developing simpler and faster design procedures while maintaining acceptable accuracy. In this case symmetries have been exploited and two particular simplified approaches have been applied, both based on the idea of modelling each magnet and each coil individually and superimposing the solutions. As a result, two algorithms have been considered, one using a 2D axisymmetric finite element (2D FE) formulation [7] and second applying directly the Biot-Savart law (BS). In both approaches it is assumed that the solution for each magnet and each coil is axisymmetric. Moreover, it is adopted that each magnet is represented by an infinitely thin cylindrical current sheet with appropriate current density representing the axial value of magnetization vector [8].

In the proposed algorithm an edge formulation of the 2D finite element method has been employed; here the unknowns are the edge values ϕ of the vector potential $\mathbf{A}$. Under the axial symmetry the edges are formed by circles $r = r_i$, $z = z_i$, whose trace on the $\psi = $ const plane are the nodes $P_i(r_i, z_i)$ of the discretization mesh. The edge value ϕ_i associated with the circle $r = r_i$, $z = z_i$ is given by a product of the circumferential component, A_Ψ, of the potential $\mathbf{A}$ and the length l_i of the circumference, i.e. $\phi_i = 2\pi r_i A_\Psi(r_i, z_i)$. In the ensuing FEM algorithm the

equations were formed separately for the coil and magnet regions. From the computed distributions of ϕ_i the radial, B_r, and axial, B_z, components of flux density were derived as functions of position ($B_r = f(r, z)$, $B_z = f(r, z)$).

The application of Biot-Savart law leads to an analytical expression, which may be treated as exact, providing the constituent elliptical functions are calculated accurately. The components of **B** and consequently distributions of $B_r = f(r, z)$ and $B_z = f(r, z)$ were derived following the approach proposed in [9], where the elliptic integrals are expressed in terms of power series and Legendre polynomials. At least 70 terms have been included in the relevant power series; such a large number (denoted k_s) was necessary because of the very small distances between the points where the flux density was sought and the positions of the sources. Several numerical tests have been conducted to estimate the minimum necessary number of terms by comparing the resultant axial forces and torques. The adopted criterion was that the results for k_s and $k_s + 100$ should not differ by more than 0.01%. An interesting outcome, however, was that due to the large value of k_s, as well as the need to treat each turn of the coil separately, the overall computing time for the Biot-Savart method was longer than for the 2D FE approach. Another algorithm was also developed to account for the helical winding [10] in the Biot-Savart equation. It was found, however, that negligible gain in accuracy was achieved while computing times were distinctly longer [7]. Therefore this algorithm has not been taken into account in the design calculations.

For both algorithms, the global solution may then be obtained by superimposing all component results, bearing in mind that it is not necessary to repeat calculations for each magnet or coil; instead two solutions only are needed, for one coil and one magnet, which then need to be scaled (according to the value of the coil current or magnetization vector) and transposed from a local to a global coordinate system.

The transformation of the components of the flux density vector **B** from the 2D axisymmetric to the 3D frame of reference is illustrated by Fig. 3. Additionally, in Fig. 4 the way illustrating the distribution transformation of the magnetic flux density components between the systems for a single magnet has been presented. Both the global and local systems use cylindrical coordinates; the global one is denoted as $R\psi Z$. The following relationships hold between the components B_R, $B\psi$ and B_Z in the global system and the local values B_r, B_z, for the j-th source and the local coordinates r_j and z_j

$$B_R(R, \psi, Z) = \sum_{j=1}^{n} B_r\left(\mid r_j \mid, z_j\right) \frac{R - r_j^{'} \cos\left(\psi - \psi_j^{'}\right)}{\sqrt{\left(r_j^{'}\right)^2 + R^2 - 2r_j^{'} R \cos\left(\psi - \psi_j^{'}\right)}}, \tag{1}$$

$$B_\Psi(R, \psi, Z) = \sum_{j=1}^{n} B_r\left(\mid r_j \mid, z_j\right) \frac{r_j^{'} \sin\left(\psi - \psi_j^{'}\right)}{\sqrt{\left(r_j^{'}\right)^2 + R^2 - 2r_j^{'} R \cos\left(\psi - \psi_j^{'}\right)}}, \tag{2}$$

$$B_Z(R, \psi, Z) = \sum_{j=1}^{n} B_z\left(\mid r_j \mid, z_j\right), \tag{3}$$

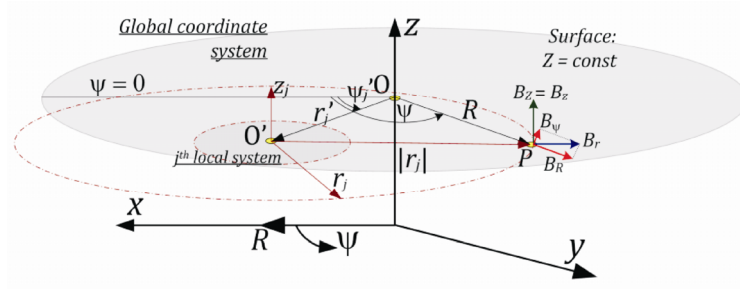where: *n* is the number of local systems, in this case the number of permanent magnets and coils.

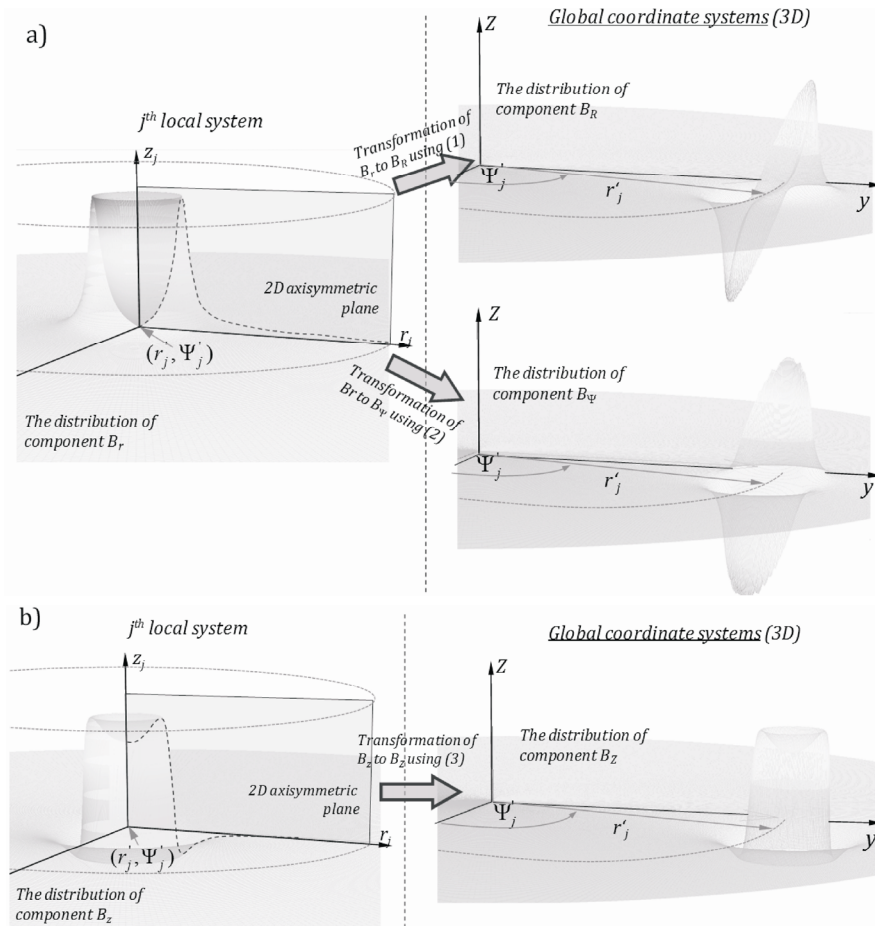Fig. 3. The global and the *j*-th local coordinate systems

Fig. 4. Transformation of distributions of magnetic flux density components from 2D local system to 3D global system: (a) component of B_r on components of B_R and $B\psi$; and (b) component of B_z on the component of B_Z

The ensuing bespoke algorithms allow the electromagnetic torque and the axial force between the stator and the rotor to be estimated; the relevant component torques and forces are calculated from the Maxwell stress formulas [11]. Finally, the derived procedures for estimating field distribution and the value of the resultant torque have been integrated into the design routines of the motor.

4. Validation of the proposed algorithms against commercial software

The author decided to evaluate the effectiveness of the proposed algorithms by comparing the obtained results with the results of simulations performed using commercial software Maxwell 3D, i.e. software, which bases on a classical FE formulation using nodal elements and magnetic scalar potential Ω. The high number of testing calculations has been performed using the developed algorithms as well as full 3D FE model. In the paper, the selected results have been given. In the Figs. 5-7, the components B_R, B_ψ and B_Z of the flux density as a function of the angle ψ along the circle of radius $R = r_s$ on the plane $Z = h_c + 0.5\delta$ have been shown. The presented results refer to a case of a motor supplied but on no-load, at the time instant when phase currents are $i_a = -i_b = 1$ A and $i_c = 0$ A, while the field axis of stator coincides with the field axis of rotor. Fig. 8 demonstrates the variation of the electromagnetic torque as a function of the angle α, i.e. angle between the stator and rotor field axes, while the phase currents are as specified above; in addition the measured torque characteristic as a function of the angle α is also included.
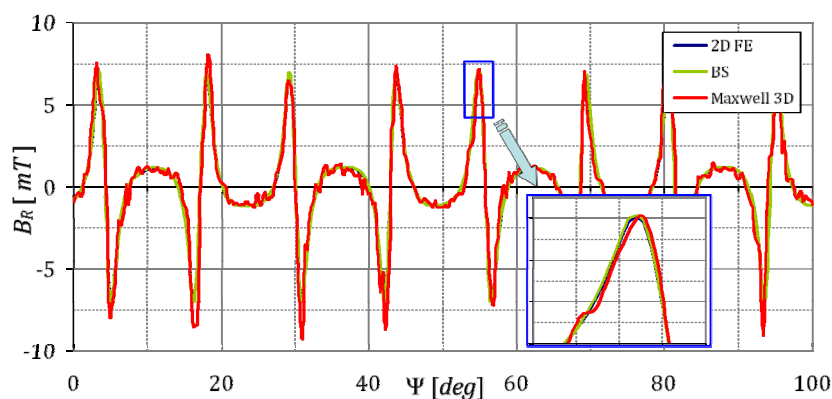

Fig. 5. The distribution of component B_R, $B_R(\psi)$ for $R = r_s$ and $Z = h_c + 0.5\delta$
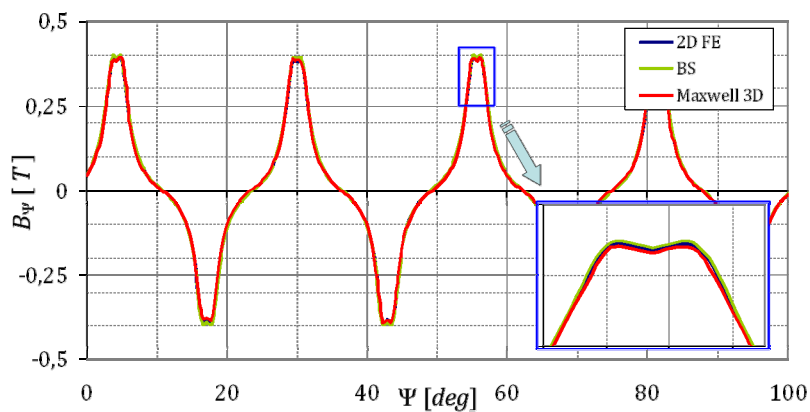
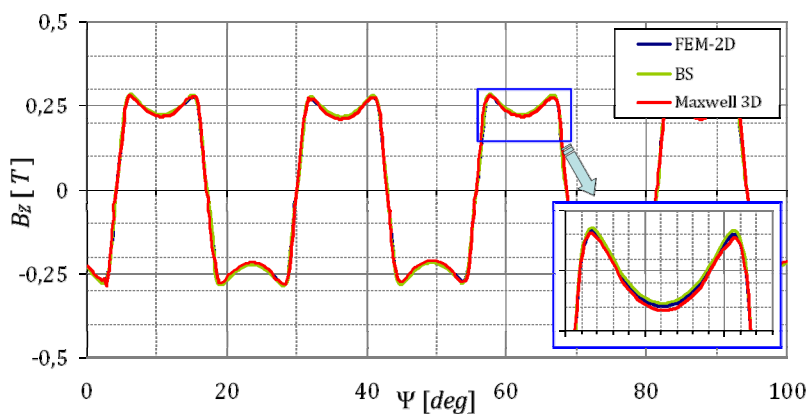Fig. 6. The distribution of component B_ψ, $B_\psi(\psi)$ for $R = r_s$ and $Z = h_c + 0.5\delta$

Fig. 7. The distribution of component B_Z, $B_Z(\psi)$ for $R = r_s$ and $Z = h_c + 0.5\delta$
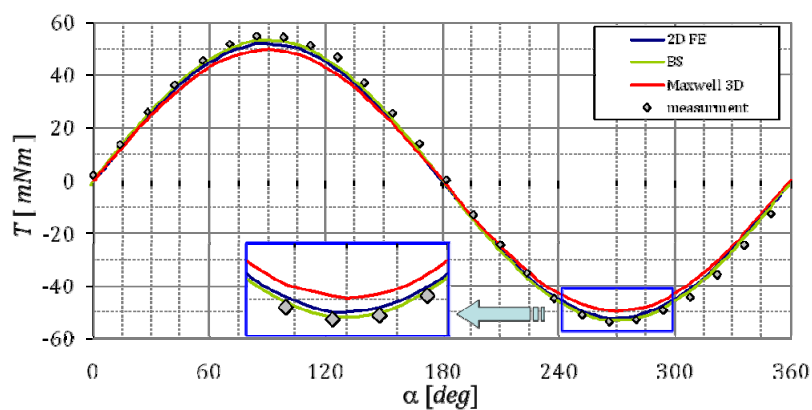

Fig. 8. Electromagnetic torque as a function of angle α

The values of magnetic flux density obtained by different methods are reasonably close to each other. The best agreement with measurement is achieved when a Biot-Savart equation is used, which was to be expected. The calculated torque then differs from the experimental value by not more than 2.1%; the 2D FE and Maxwell 3D results show inaccuracies of 4.1% and 8.5%, respectively.

The most interesting and significant findings, however, are related to the computational effort. Using a particular computer, a single FE solution for the 2D axisymmetric model (for one coil or one permanent magnet) takes just under 5 s; the relevant figure when the Biot-Savart equation is used is 22 s. The full 3D simulation with Maxwell 3D required 83 minutes. It is also worth noting that subsequent calculations with 2D FE or via Biot-Savart law – for example for another value of the angle α or a different current – require less time; this is because field distributions do not need to be recalculated (only transformations are applied). Another difference is the fact that when using the proposed superposition techniques always the whole motor was considered, whereas when using Maxwell 3D symmetries were sought (to reduce the computational effort) and in practice only part of the motor's circumference was considered for meshing (in the particular case it was 2/7th of the machine). Overall more than 1.5 million of elements were required, even with the mentioned symmetries accounted for, in order to achieve reasonably smooth electromagnetic torque variation and reduce the effects of discretization on the accuracy of the solution. The relative residual in the Maxwell 3D software was set at 10^{-3}%.

5. The design optimisation of AFPMC motor

The main purpose of the proposed algorithms, which rely on superposition and 2D field modelling techniques, was to incorporate them into the design optimisation systems, where re-ducing the time required for a single objective function evaluation is of paramount practical importance. This was indeed the motivation behind this study, to develop accurate (in com-parison with full 3D simulations) but much faster models which would be suitable for design purposes. This has been accomplished by combining the algorithms with an in-house design system utilizing a genetic algorithm [12].

The optimisation task had been defined as explained below. The following dimensions were fixed: the distance between the centers of the coils and the magnets $r_s = 45$ mm (see Fig. 1), the air-gap $\delta = 1$ mm, the thickness of the stator and rotor plates 1.5 mm, the inner diameter of a coil 3.8 mm, and the height $h = h_c + h_m + \delta \leq h_z$ ($h_z = 12.5$ mm). The optimal design was then searched for such a set of design parameters s for which the AFPMC motor would have the highest value of k_T, the ratio of the average torque T_{av} to the mass of the magnets m_{pm}, with a constraint that $T_{av} \geq T_z$ ($T_z = 50$ mNm). The average torque was computed for one operating cycle of the motor under the BLDC control mode, while the current density was assumed to be $J = 6$ A/mm^2 because of the class of the insulation used. The vector of the design parameters s was assumed to include: the magnet radius r_m, the magnet height h_m, the outer diameter r_c and the height h_c of the coils; hence. The objective function was defined as

$$f_i(\boldsymbol{s}) = k_{T,i}(\boldsymbol{s}) / \overline{k}_T^0 , \tag{4}$$

where $k_{T,i}(\boldsymbol{s})$ is the ratio of the average torque T_{av} to the mass of the magnets m_{pm} for the i-th 'individual' from the n-th population, while $\overline{k}_T^0$ is the highest value of k_T attained during the initialization stage. The inequality constraints included the desired average torque $T_{av} \geq T_z$ and the limitation on the height $h \leq h_z$. The optimisation task was therefore supplemented by penalty functions resulting in the following modified objective function $h_i^{(m)}(\boldsymbol{s})$

$$h_i^{(m)}(\boldsymbol{s}) = f_i(\boldsymbol{s}) \cdot e^{-g_i^{(m)}(\boldsymbol{s})} \cdot e^{-p_i^{(m)}(\boldsymbol{s})} , \tag{5}$$

where the functions $g_i^{(m)}(\boldsymbol{s})$ and $p_i^{(m)}(\boldsymbol{s})$ describe the modified penalty functions specified according to the rules set out in [12], i.e.

$$g_i^{(m)}(\boldsymbol{s}) = \begin{cases} 0 & \text{for } T_{av,i}(\boldsymbol{s}) \geq T_z \\ r^{(m)} f_i^{-1}(s)\left(T_z - T_{av,i}(\boldsymbol{s})\right) T_z^{-1} & \text{for } T_{av,i}(\boldsymbol{s}) < T_z \end{cases} , \tag{6}$$

$$p_i^{(m)}(\boldsymbol{s}) = \begin{cases} 0 & \text{for } h_i(\boldsymbol{s}) \leq h_z \\ r^{(m)} f_i^{-1}(s)\left(h_i(\boldsymbol{s}) - h_z\right) h_z^{-1} & \text{for } h_i(\boldsymbol{s}) > h_z \end{cases} , \tag{7}$$

where $r > 1$ is the penalty coefficient, m is the number of penalty iterations, $T_{av,i}(\boldsymbol{s})$ and $h_i(\boldsymbol{s})$ denote the average torque T_{av} and the height h of the i-th individual, respectively.

The following genetic algorithm parameters were assumed: 500 individuals in a population, the mutation coefficient of 0.5% and the maximum number of generations of 50. In addition, the iterations were allowed to terminate sooner if the ratio of the modified average fitness h_{av} of the n-th population to the value of the modified objective function for the best individual h_{max} were to exceed 0.98. For the optimisation task defined as above the total computing time for the case when field distributions and torque characteristics were estimated using the 2D FE model was around 12 hours, whereas when the Biot-Savart equation was used it was about 32 hours.

The results are summarized in Table 1, showing intermediate sets of parameters after a certain number of iterations. The process actually terminated after 26 generations.

Table 1. Optimisation of the AFPMC motor using the Biot-Savart equation
for evaluation of fields and electromagnetic torque

	r_m	h_m	r_c	h_c	k_T	T_{av}	h_{av}	h_{max}	$f_i(h_{max})$
No.	mm	mm	mm	mm	mNm/g	mNm	–	–	–
1	4.3	1.7	6.6	9.6	2.353	48.8	0.431	0.854	0.887
10	4.4	1.9	6.6	9.7	2.238	54.3	0.523	0.806	0.843
20	4.5	1.7	6.5	9.7	2.276	51.7	0.726	0.857	0.857
26	4.5	1.6	6.6	9.9	2.395	51.2	0.881	0.898	0.898

The values of the four design parameters are shown (r_m, h_m, r_c, h_c), as well as the average torque T_{av}, the ratio k_T, the modified objective function (h_{max}) for the best individual; the

modified average fitness (h_{av}) for the *n*-th population, and the value of the objective function $f_i(h_{max})$ of the individual for which the modified objective function accepts the max value. The field distributions were obtained using the Biot-Savart approach. It was also assumed that the design parameters will be evaluated with an accuracy of 0.1 mm.

As a result of this optimisation a decision was taken to build an AFPMC motor of the following dimensions: r_m = 4.5 mm, h_m = 1.6 mm, r_c = 6.6 mm and h_c = 9.9 mm. The values of these design parameters have been used when determining of the distributions of magnetic flux density components presented in Figs. 5-7 and the calculating of the moment characteristics included in Fig. 8.

6. Conclusions

In the paper, the comparison between the commonly applied approach using 3D FEA and the proposed approach using the superposition of axisymmetric 2D solutions for the analysis of the coreless systems has been carried out. The superiority of the presented method has been demonstrated on the case study problem. In the author's opinion the approach of using the superposition principle offers a very efficient methodology for practical design, far superior in the view of significantly reduced computing times and competitive in terms of accuracy in relation to the 3D FE modeling. The numerical technique, presented in the paper, is particularly appropriate in the optimisation of discussed coreless systems as the time for a single evaluation of an objective function may be reduced significantly, thus allowing for more thorough design space exploration and a much higher number of the cases studied.

References

[1] Lovatt H.C., Ramsden V.S., Mecrow B.C., *Design of an in-wheel motor for a solar-powered electric vehicle*, IEE Proceedings – Electric Power Applications 145(5): 402-408 (1998).

[2] Dong J., Huang Y., Shen P., Jin L., Ge B., *An axial flux flywheel motor/generator for pulsed power application*, Proc. IEEE Energy Conversion Congress and Exposition (ECCE 2012), Raleigh, NC, pp. 678-683 (2012).

[3] Bumby J.R., Martin R., *Axial-flux permanent magnet air-cored generator for small scale wind turbines*, IEE Proceedings – Electric Power Applications 152(5): 1065-1075 (2005).

[4] Gieras J., Wang R., Kamper M., *Axial flux permanent magnet brushless machine*, 2nd Edition, Springer (2008).

[5] Judge A., *Permanent magnet axial field air core (PAAC) motors for naval applications*, Proc. ASNE Elect. Mach. Technol. Symposium, Philadelphia, USA, pp. 46-53 (2012).

[6] http://www.katech.com/katfiles/sema.html, accessed December 2015.

[7] Boczkowski T., Demenko A., Wojciechowski R.M., Sykulski J.K., *Applying superposition of 2D results to model 3D field distributions in magnetically linear devices using an example of an axial flux permanent magnet coreless motor*, Proc. Compumag, Montreal, Canada, 2pp (2015).

[8] Demenko A., Stachowiak D., *Representation of permanent magnets in the 3-D finite element description of electrical machines,* Electromotion 14(1): 3-9 (2007).

[9] Smythe W.R., *Static and dynamic electricity*, 2nd ed., McGraw – Hill Book Company (1950).

[10] Budnik K., Machczyński W., *Magnetic field of complex helical conductors*, Archives of Electrical Engineering 62(4): 533-540 (2013).

[11] Demenko A., Łyskawiński W., Wojciechowski R.M., *Equivalent formulas for global magnetic force calculation from finite element solution*, IEEE Transactions on Magnetics 48(2): 195-198 (2012).

[12] Knypinski Ł., Nowak L., *Optimization of the permanent magnet brushless DC motor employing finite element method*, Compel 32(4): 1189-1202 (2013).